

# Exact Solution of the Frustrated Potts Model with Next-Nearest-Neighbor Interactions in One Dimension: An AI-Aided Discovery

Weiguo Yin\*

Condensed Matter Physics and Materials Science Division,  
Brookhaven National Laboratory, Upton, New York 11973, USA

(Dated: April 8, 2025)

The one-dimensional  $J_1$ - $J_2$   $q$ -state Potts model is solved exactly for arbitrary  $q$  by introducing the maximally symmetric subspace (MSS) method to analytically block diagonalize the  $q^2 \times q^2$  transfer matrix to a simple  $2 \times 2$  matrix, based on using OpenAI's latest reasoning model `o3-mini-high` to exactly solve the  $q = 3$  case. It is found that the model can be mapped to the 1D  $q$ -state Potts model with  $J_2$  acting as the nearest-neighbor interaction and  $J_1$  as an effective magnetic field, extending the previous proof for  $q = 2$ , i.e., the Ising model. The exact results provide insights to outstanding physical problems such as the stacking of atomic or electronic orders in layered materials and the formation of a  $T_c$ -dome-shaped phase often seen in unconventional superconductors. This work is anticipated to fuel both the research in one-dimensional frustrated magnets for recently discovered finite-temperature application potentials and the fast moving topic area of AI for sciences.

Finding novel phases and phase transitions is a central challenge in various research fields, including condensed matter physics, materials science, quantum information, and micro-electronics [1]. Unusual phases abound in frustrated magnets [2], which are described typically by the Ising model [3] or the quantum Heisenberg model [4] with competing spin-spin interactions either in the form of an equilateral triangle or via competition between the nearest-neighbor (NN) interaction  $J_1$  and next-nearest-neighbor (NNN) interaction  $J_2$  [1].

The third basic model of statistical mechanics is the  $q$ -state Potts model [5–8], which is a generalization of the Ising model ( $q = 2$ ) and can serve as a useful intermediary to study the transition from discrete (Ising) to continuous (Heisenberg) symmetry. In particular, the one-dimensional (1D)  $J_1$ - $J_2$  Potts model could be relevant to problems ranging from the out-of-plane stacking of atomic or electronic orders in layered materials, such as charge stripe ordering in  $\text{La}_{1.67}\text{Sr}_{0.33}\text{NiO}_4$  [9], the Star-of-David charge-density wave in  $1T$ - $\text{TaS}_2$  [10], and spin spiral ordering in the Weyl semimetal  $\text{EuAuSb}$  [11], to a time series with multiple choices at every time step such as table tennis training drill designs.

While the  $J_1$ - $J_2$  Ising model and Heisenberg model in one dimension [12–15] and two dimension [16–18] have been extensively studied, only the 1D  $J_1$ - $J_2$  Ising model has been solved exactly by using the transfer matrix method [19]. Exact analytic solutions of the 1D  $J_1$ - $J_2$  Potts model also remain unknown; since the model with  $q = 3$  already exhibits a distinct ground-state phase behavior from that with  $q = 2$ , i.e., the Ising model (Fig. 2) [11], it is of fundamental importance to exactly solve the model for arbitrary  $q$ . The challenge arises from rapid increase in the order of the transfer matrix, which equals  $q^2$ . No wonder a  $9 \times 9$  matrix for  $q = 3$  is already hard to solve analytically and diagonalization of a  $(10^{10})^2 \times (10^{10})^2$  matrix for  $q = 10^{10}$  is simply beyond reach even numerically. Previous studies remarkably reduced the task to numerical calculations for an effective  $q \times q$  matrix in the integer- $q$  formalism of the transfer matrix—and for an effective  $2 \times 2$  matrix in the continuous- $q$  formalism

of the transfer matrix where physics is less transparent—however, short of analytic exact results [20]. Hence, an intuitive understanding of the rich phase behaviors in the 1D  $J_1$ - $J_2$  Potts model is still lacking.

Two recent developments shed light on this long-standing problem. The first one is the analytic reduction of the  $4 \times 4$  transfer matrix for a decorated Ising ladder to an effective  $2 \times 2$  matrix using symmetry-based block diagonalization, leading to the discovery of spontaneous finite-temperature ultranarrow phase crossover (UNPC), which exponentially approaches the forbidden finite-temperature phase transition in 1D Ising models [21], and the subsequent discovery of in-field UNPC driven by exotic ice-fire states [22–24]. These findings point out the promising potentials of 1D frustrated magnets in finite-temperature applications; finding exact solutions for 1D frustrated Potts model could define a milestone in this important new direction. The second development is the derivation of an elegant equation—that determines the critical temperature of UNPC in site-decorated Ising models in an external magnetic field—by OpenAI's latest reasoning model `o3-mini-high` at the first-ever 1000-Scientist AI Jam Session [24]. Hence, the author was inspired to prompt this AI reasoning model progressively to handle the transfer matrix in the integer- $q$  formalism for the  $q = 3$  case—despite quite a few errors in AI's responses—and eventually have found a symmetry-based block diagonalization that can analytically reduce the  $9 \times 9$  transfer matrix of the 1D  $J_1$ - $J_2$  three-state Potts model to an effective  $2 \times 2$  matrix.

For general  $q$ , the key symmetry is the full permutation symmetry of the  $q$  Potts states. In other words, the Hamiltonian (and therefore the transfer matrix in the integer- $q$  formalism) is invariant under any permutation of the labels  $\{1, 2, 3, \dots, q\}$ ; its symmetry group is  $\mathcal{S}_q$ . Although the AI failed to go further but warned that the number of permutations increases dramatically as  $q$  increases, the exact results for the  $q = 2$  and 3 cases—especially the point that both arrive at an effective  $2 \times 2$  matrix—stimulated the author to realize that since only the largest eigenvalue ( $\lambda$ ) of the transfer matrix matters in the thermodynamic limit, the task is reduced

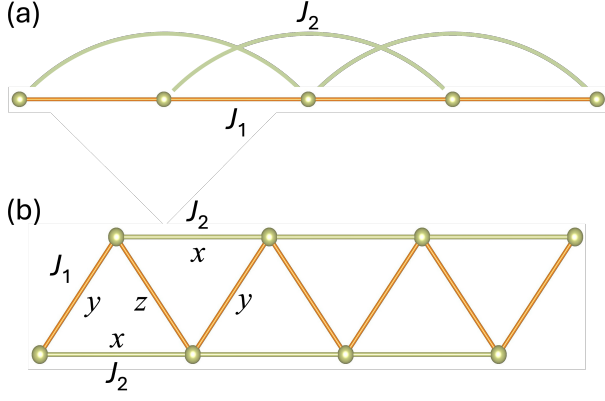


FIG. 1. Schematics of (a) the single-chain  $J_1 - J_2$  Potts model [6] and (b) its equivalent zigzag-ladder representation. The balls stand for the spins with  $q$  states. The orange bonds stand for the nearest-neighbor interactions  $J_1$  and the greenish bonds stand for the next-nearest-neighbor interactions  $J_2$ . The contribution of each bond to the partition function is  $x = e^{\beta J_2}$ ,  $y = e^{\beta J_1/2}$ , or  $z = e^{\beta J_1} = y^2$  when its two end spins are the same, and one otherwise.

to identify the symmetry-separated subspace that contains  $\lambda$ . Then, the author found that this subspace is spanned by two maximally symmetric vectors because all the transfer matrix elements are positive, resulting in an analytic  $2 \times 2$  matrix. Therefore, the surprisingly simple exact solution of the 1D  $J_1 - J_2$  Potts model has been obtained for arbitrary  $q$ .

We consider the following Hamiltonian [Fig. 1(a)]

$$H = -J_1 \sum_{i=1}^{2N} \delta(\sigma_i, \sigma_{i+1}) - J_2 \sum_{i=1}^{2N} \delta(\sigma_i, \sigma_{i+2}), \quad (1)$$

where  $\sigma_i \in \{1, 2, 3, \dots, q\}$  is the spin variable at site  $i$ .  $\delta(\sigma_i, \sigma_{i+1})$  is the Kronecker delta (which equals 1 if  $\sigma_i = \sigma_{i+1}$  and 0 otherwise).  $2N$  is the total number of the spins with  $\sigma_{2N+1} \equiv \sigma_1$  and  $\sigma_{2N+2} \equiv \sigma_2$ , viz., the periodic boundary condition.

To construct the transfer matrix, we use both the overlapping-pairs formulation for Equation (1) with one spin per unit cell to get  $\mathbb{T}$  and the equivalent zigzag ladder version of the model with two spins per unit cell [Fig. 1(b) and Equation (S1) in End Matter A] to obtain  $\mathbb{T}'$ ; they satisfy  $\mathbb{T}' = \mathbb{T}^2$ . In the thermodynamic limit  $N \rightarrow \infty$ , the partition function  $Z = \text{Tr} e^{-\beta H} = \lambda^{2N}$ , where  $\lambda$  is the largest eigenvalue of the transfer matrix  $\mathbb{T}$ . The free energy per spin is given by

$$f = \lim_{N \rightarrow \infty} -\frac{1}{2N\beta} \ln Z = -\frac{1}{\beta} \ln \lambda, \quad (2)$$

where  $\beta = 1/(k_B T)$  with  $T$  being the absolute temperature and  $k_B$  the Boltzmann constant.  $f$  determines physical properties such as the entropy per spin  $S = -\partial f / \partial T$ , the specific heat  $C_v = T \partial S / \partial T$ , the NN correlation  $\langle \delta(\sigma_i, \sigma_{i+1}) \rangle = -\partial f / \partial J_1$ , the NNN correlation  $\langle \delta(\sigma_i, \sigma_{i+2}) \rangle = -\partial f / \partial J_2$ , and the energy per spin  $E = -\partial f / \partial \beta = -J_1 \langle \delta(\sigma_i, \sigma_{i+1}) \rangle - J_2 \langle \delta(\sigma_i, \sigma_{i+2}) \rangle$ .

The  $\lambda$ -containing subspace is spanned by the following two maximally symmetric  $q^2 \times 1$  vectors:

$$|\psi_1\rangle = \frac{1}{\sqrt{q}} \sum_{s=1}^q \sum_{s'=1}^q \delta(s, s') |s, s'\rangle, \\ |\psi_2\rangle = \frac{1}{\sqrt{q^2 - q}} \sum_{s=1}^q \sum_{s'=1}^q [1 - \delta(s, s')] |s, s'\rangle. \quad (3)$$

The resulting transformation matrix  $U_{q^2} = \{|\psi_1\rangle, |\psi_2\rangle\}$  is a  $q^2 \times 2$  matrix that projects the  $q^2 \times q^2$  transfer matrix  $\mathbb{T}$  to the  $2 \times 2$  block  $\mathbb{T}_2 = U_{q^2}^T \mathbb{T} U_{q^2}$ , which is decoupled from the rest thanks to different symmetry and given by

$$\mathbb{T}_2 = \begin{pmatrix} u & w \\ w & v \end{pmatrix} = \begin{pmatrix} xy^2 & \sqrt{q-1}y \\ \sqrt{q-1}y & x + q - 2 \end{pmatrix} \quad (4)$$

with the shorthand notations  $x = e^{\beta J_2}$  and  $y = e^{\beta J_1/2}$ . Note that the maximally symmetric subspace means that the expressions of  $u$ ,  $v$ , and  $w$  can be obtained straightforward by combinatorial analysis. The largest eigenvalue of  $\mathbb{T}$  is the larger eigenvalue of  $\mathbb{T}_2$  and is given by

$$\lambda = \frac{u+v}{2} + \sqrt{\left(\frac{u-v}{2}\right)^2 + w^2}. \quad (5)$$

Equation (4) is the same as the projected transfer matrix for the 1D  $q$ -state Potts model with  $J_2$  acting as the NN interaction and  $J_1$  as an effective magnetic field [25]

$$H_{\text{eff}} = -J_2 \sum_{i=1}^{2N} \delta(\sigma_i, \sigma_{i+1}) - J_1 \sum_{i=1}^{2N} \delta(\sigma_i, 1), \quad (6)$$

in the maximally symmetric subspace of its  $q \times q$  transfer matrix, expanded by the following two  $q \times 1$  vectors:

$$|\phi_1\rangle = \sum_{s=1}^q \delta(s, 1) |s\rangle, \\ |\phi_2\rangle = \frac{1}{\sqrt{q-1}} \sum_{s=1}^q [1 - \delta(s, 1)] |s\rangle. \quad (7)$$

This mapping was proven for the 1D  $J_1 - J_2$  Ising model ( $q = 2$ ) using the substitution of  $\tau_i = \sigma_i \sigma_{i+1}$  and  $\tau_i \tau_{i+1} = \sigma_i \sigma_{i+2}$  where  $\sigma_i = \pm 1$  is the Ising spin values [12, 13]. It is now proven to apply to arbitrary  $q$ .

The simplicity of Equation (4) provides an intuitive understanding of rich phase behaviors in the 1D  $J_1 - J_2$  Potts model. We are interested in frustrated cases where  $J_2 < 0$  is antiferromagnetic and have set  $-J_2 = 1$  as the energy unit from now on. The  $q$ -dependent phase diagrams given by the normalized entropy  $2S(J_1, T) / \ln q$  are shown in Fig. 2. A  $T_c$ -dome-like phase emerges at low temperature for small  $q$  and disappears for large  $q$ . The phase diagrams given by  $\langle \delta(\sigma_i, \sigma_{i+1}) \rangle$  and  $\langle \delta(\sigma_i, \sigma_{i+2}) \rangle$  are shown in Fig. S1 in End Matter.

To get insights to these rich phase diagrams, we start with analyzing ground-state phase behaviors. At  $T = 0$ , the 1D

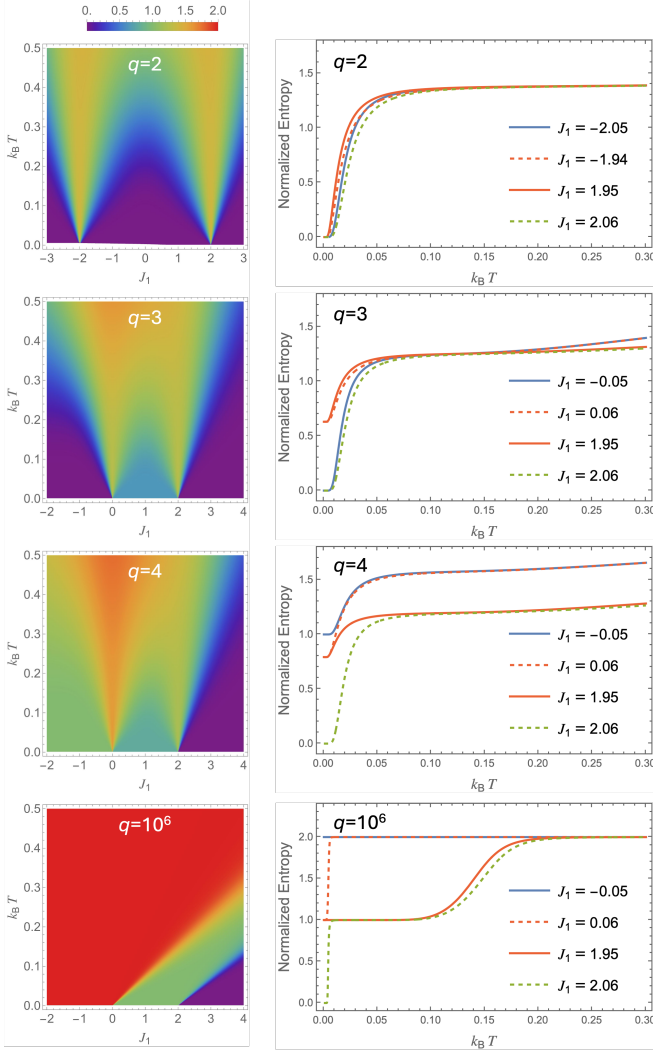


FIG. 2. Phase diagrams for  $q = 2, 3, 4$ , and  $10^6$ . Left panels: Density plots of the normalized entropy  $2S(J_1, T)/\ln q$  in the  $J_1 - T$  plane. Right panels: The temperature dependence of  $2S(J_1, T)/\ln q$  for selected  $J_1$  values around the critical points.  $-J_2 = 1$  is set as the energy unit.

$J_1$ - $J_2$  Potts model for all  $q$  values have three phases separated by two critical points (CPs), determined by the relative magnitude of  $u, w, v$  in Equation (4). The right-hand-side phase for  $J_1 > 2$  (where  $u$  dominates) is always “ferromagnetic” with  $\langle \delta(\sigma_i, \sigma_{i+1}) \rangle = \langle \delta(\sigma_i, \sigma_{i+2}) \rangle = 1$  and  $E = -J_1 - J_2$ ; more precisely, it is a mixture of  $q$  ferromagnetic states, i.e.,  $\frac{1}{\sqrt{q}}(|111\dots\rangle + |222\dots\rangle + \dots + |qqq\dots\rangle)$ . The “ferromagnetic transition” CP at  $J_1 = 2$  has a residual entropy per spin

$$S(J_1 = 2, T = 0) = \ln \left( \frac{1 + \sqrt{4q - 3}}{2} \right). \quad (8)$$

The  $q = 2$  case (i.e., the Ising model) differs from the  $q \geq 3$  cases in two aspects: (i) the two CPs for  $q = 2$  are symmetry related and located at  $J_1 = \pm 2$ , while they are located at  $J_1 = 0$  and  $2$  for  $q \geq 3$ . (ii) None of the three phases for  $q = 2$

has a macroscopic degeneracy, while one or two nontrivial states with residual entropy exist for  $q \geq 3$ . These phases and CPs will be elaborated in passing. Concerning the spin configurations in one dimension, we adopt the convention that the spins are arranged from left to right from now on.

$q = 2$ : The  $J_1 > 0$  and  $J_1 < 0$  regions are symmetry related by flipping the spins on one sublattice. Consequently, the left-hand-side phase for  $J_1 < -2$  is “antiferromagnetic” with  $\langle \delta(\sigma_i, \sigma_{i+1}) \rangle = 0$ ,  $\langle \delta(\sigma_i, \sigma_{i+2}) \rangle = 1$ ,  $E = -J_2$ . The two CPs are located at  $J_1 = \pm 2$ . The CP at  $J_1 = -2$  has the same residual entropy as that at  $J_1 = 2$  given by Equation (8), i.e.,  $\ln(\frac{1+\sqrt{5}}{2})$ , which is indeed the same as the magnetic-field-induced CP in the 1D Ising model with only NN interactions [26]. The middle phase for  $-2 < J_1 < 2$  is a dimerized state, i.e., a pair of NN spins have the same variable but differ from the last pair, forming the patterns of ...11221122... and its three degenerate shifts, leading to  $\langle \delta(\sigma_i, \sigma_{i+1}) \rangle = 1/2$ ,  $\langle \delta(\sigma_i, \sigma_{i+2}) \rangle = 0$ , and  $E = -J_1/2$ . None of the three phases has a macroscopic degeneracy.

$q \geq 3$ : The middle phase for  $0 < J_1 < 2$  (where  $w$  dominates) is a randomly dimerized state (RDS) with  $\langle \delta(\sigma_i, \sigma_{i+1}) \rangle = 1/2$ ,  $\langle \delta(\sigma_i, \sigma_{i+2}) \rangle = 0$ , and  $E = -J_1/2$ , where like in the dimerized phase for  $q = 2$ , a pair of NN spins have the same variable but differ from the last pair, so it has  $q - 1$  choices, yielding a residual entropy of  $\ln(q - 1)$  per two spins or  $\ln \sqrt{q - 1}$  per spin. This phase could be relevant to the stacking problem of the Star-of-David charge-density wave in  $1T$ -TaS<sub>2</sub> [10]. The left-hand-side phase for  $J_1 < 0$  (where  $v$  dominates) is a paramagnet with  $\langle \delta(\sigma_i, \sigma_{i+1}) \rangle = \langle \delta(\sigma_i, \sigma_{i+2}) \rangle = 0$  and  $E = 0$ , where any spin differs from the two last spins, so it has  $q - 2$  choices, yielding a residual entropy of  $\ln(q - 2)$  per spin; notably,  $q = 3$  is special since the residual entropy is zero, forming the patterns of ...123123... and its five degenerate states by permutations of  $\{1, 2, 3\}$ , reminiscent of the ABC stacking pattern of the charge stripe order in La<sub>1.67</sub>Sr<sub>0.33</sub>NiO<sub>4</sub> [9] and the 120° spin spiral order in the Weyl semimetal EuAuSb [11]. In the CP at  $J_1 = 0$ , any spin differs from its last next-nearest neighbor, so it has  $q - 1$  choices, yielding a residual entropy of  $\ln(q - 1)$  per spin; again,  $q = 3$  is special because its residual entropies at both CPs are equal to  $\ln 2$ .

The  $q$  dependence of the residual entropies for the left and middle phases as well as the two CPs is summarized in Fig. 3. For small  $q$ , the residual entropies of the CPs (dashed lines) are considerably larger than those of their adjacent phases (solid lines). Consequently, each CP develop a V-shape region in the  $J_1 - T$  phase diagram as  $T$  increases (Fig. 2, left panels for  $q = 2, 3, 4$ ). The V-shape regions of the two CPs join to create a  $T_c$ -dome-like region for the middle randomly dimerized phase for  $q \geq 3$ . When placed near the CPs, the system does not follow the common lore—i.e., transition to the adjacent phase with higher macroscopic degeneracy—but transitions to the CP-developed V-shape region, also shown as the flat region in the  $T$  curve of the entropy (Fig. 2, right panels for  $q = 2, 3, 4$ ), where the entropy value equals the corresponding CP’s residual entropy.

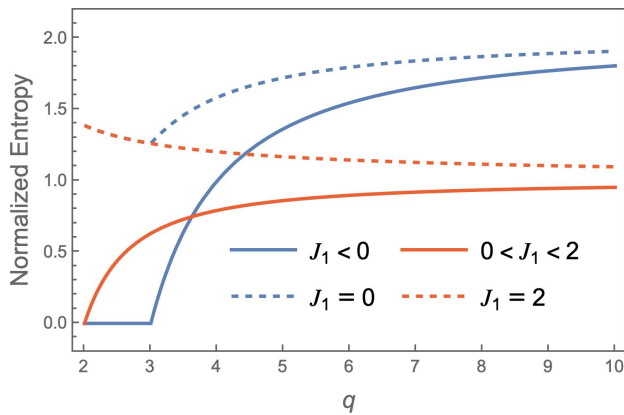


FIG. 3. The  $q \geq 3$  dependence of the zero-temperature normalized entropy  $2S(J_1, 0)/\ln q$  for four different regions of  $J_1$ :  $S = \ln(q - 2)$  for  $J_1 < 0$ ,  $S = \ln(q - 1)$  for  $J_1 = 0$ ,  $S = \ln \sqrt{q - 1}$  for  $0 < J_1 < 2$ , and  $S = \ln[(1 + \sqrt{4q - 3})/2]$  for  $J_1 = 2$ . The  $q = 2$  case, which need be specially treated for different  $J_1$  regions (see text), was added for comparison.  $J_2 = -1$ .

On the other hand, Fig. 3 reveals that for large  $q$ , the residual entropies of the CPs (dashed lines) approach those of one of their adjacent phases (solid lines), becoming indistinguishable—no more V-shaped CP regions (Fig. 2, left panel for  $q = 10^6$ ). When placed near a phase boundary, the system appears to follow the common lore, i.e., transition to the adjacent phase with higher macroscopic degeneracy. In particular, the low-temperature ferromagnetic phase for  $J_1 > 2$  would undergo a two-step phase crossover, first to the middle randomly dimerized phase at  $k_B T \approx (J_1 + 2J_2)/\ln q$  and then to the left paramagnetic phase at  $k_B T \approx J_1/\ln q$ .

The  $T_c$  dome is a key phenomenon in unconventional superconductivity in cuprates, iron-based superconductors, twisted bilayer graphene, etc. [27]. It has been explained in the picture of (i) a preformed order with phase coherence gradually building up [28] or (ii) two competing phases [29]. The present  $q$ -dependent emerging and vanishing of a dome-like structure, controlled by the relative strength of the residual entropies of the phase's two CPs, provides another possibility for forming a dome-shaped phase.

In summary, the 1D  $J_1$ - $J_2$   $q$ -state Potts model has been solved exactly by discovering that the largest eigenvalue of the  $q^2 \times q^2$  transfer matrix lives in a  $2 \times 2$  maximally symmetric subspace, and found to be equivalent to the 1D  $q$ -state Potts model with  $J_2$  acting as the NN interaction and  $J_1$  as the magnetic field. The model's ground state are found to feature three phases separated by two critical points for all  $q$  values. The relative strength of the two critical points' residual entropies is large and small for small and large  $q$ , respectively, leading to the emerging and vanishing of a dome-shaped randomly dimerized phase for small and large  $q$ , respectively, providing a new mechanism for forming a dome-shaped phase. Moreover, the exact results provide insight to the stacking problems of atomic or electronic orders in layered materials. The

maximally symmetric subspace method is anticipated to offer a significant advantage over previous numerical methods as the range of interactions increases, which will be addressed in subsequent publications. These discoveries were based on using OpenAI's latest reasoning model o3-mini-high to exactly solve the  $q = 3$  case, which embodies a new paradigm of data- and value-driven discovery, inspiring scientists to evaluate and connect insights drawn from the vast—though imperfect—information provided by AI.

Brookhaven National Laboratory was supported by U.S. Department of Energy (DOE) Office of Basic Energy Sciences (BES) Division of Materials Sciences and Engineering under contract No. DE-SC0012704.

\* wyin@bnl.gov

- [1] S. A. Kivelson, J. M. Jiang, and J. Chang, *Statistical Mechanics of Phases and Phase Transitions* (Princeton University Press, Princeton, NJ, 2024).
- [2] A. P. Ramirez, Strongly geometrically frustrated magnets, *Annual Review of Materials Research* **24**, 453 (1994).
- [3] E. Ising, Beitrag zur theorie des ferromagnetismus (contribution to theory of ferromagnetism), *Zeitschrift für Physik* **31**, 253 (1925).
- [4] W. Heisenberg, On the theory of ferromagnetism, *Z. Physik* **49**, 619 (1928).
- [5] R. B. Potts, Some generalized order-disorder transformations, *Mathematical Proceedings of the Cambridge Philosophical Society* **48**, 106 (1952).
- [6] F. Y. Wu, The potts model, *Rev. Mod. Phys.* **54**, 235 (1982).
- [7] D. C. Mattis and R. Swendsen, *Statistical Mechanics Made Simple*, 2nd ed. (World Scientific, Singapore, 2008).
- [8] R. J. Baxter, *Exactly Solved Models in Statistical Mechanics* (Academic Press, 1982).
- [9] A. M. M. Abeykoon, E. S. Božin, W.-G. Yin, G. Gu, J. P. Hill, J. M. Tranquada, and S. J. L. Billinge, Evidence for short-range-ordered charge stripes far above the charge-ordering transition in  $\text{La}_{1.67}\text{Sr}_{0.33}\text{NiO}_4$ , *Phys. Rev. Lett.* **111**, 096404 (2013).
- [10] S.-H. Lee, J. S. Goh, and D. Cho, Origin of the insulating phase and first-order metal-insulator transition in  $1T$ - $\text{TaS}_2$ , *Phys. Rev. Lett.* **122**, 106404 (2019).
- [11] J. Sears, J. Yao, W. Tian, N. Aryal, W. Yin, A. M. Tsvelik, I. A. Zaliznyak, Q. Li, and J. M. Tranquada, *EuAuSb: An incommensurate helical variation on an altermagnet*, to be published (2025).
- [12] J. F. Dobson, Many-Neighbored Ising Chain, *J. Math. Phys.* **10**, 40 (1969).
- [13] J. Stephenson, Two one-dimensional ising models with disorder points, *Canadian Journal of Physics* **48**, 1724 (1970).
- [14] A. Fleszar, J. Glazer, and G. Baskaran, A complex short-range order phase diagram in a one-dimensional spin model, *Journal of Physics C: Solid State Physics* **18**, 5347 (1985).
- [15] S. R. White and I. Affleck, Dimerization and incommensurate spiral spin correlations in the zigzag spin chain: Analogies to the kondo lattice, *Phys. Rev. B* **54**, 9862 (1996).
- [16] A. A. Gangat, Weak first-order phase transitions in the frustrated square lattice  $J_1 - J_2$  classical ising model, *Phys. Rev. B* **109**, 104419 (2024).
- [17] P. Chandra, P. Coleman, and A. I. Larkin, Ising transition in frustrated heisenberg models, *Phys. Rev. Lett.* **64**, 88 (1990).

- [18] C. Roth, A. Szabó, and A. H. MacDonald, High-accuracy variational monte carlo for frustrated magnets with deep neural networks, *Phys. Rev. B* **108**, 054410 (2023).
- [19] H. A. Kramers and G. H. Wannier, Statistics of the two-dimensional ferromagnet. part I, *Phys. Rev.* **60**, 252 (1941).
- [20] Z. Glumac and K. Uzelac, Critical behaviour of the 1d q-state potts model with long-range interactions, *Journal of Physics A: Mathematical and General* **26**, 5267 (1993).
- [21] W. Yin, Paradigm for approaching the forbidden spontaneous phase transition in the one-dimensional Ising model at a fixed finite temperature, *Phys. Rev. Res.* **6**, 013331 (2024).
- [22] W. Yin and A. M. Tsvelik, Phase switch driven by the hidden half-ice, half-fire state in a ferrimagnet, *Phys. Rev. Lett.* **133**, 266701 (2024).
- [23] W. Yin, Paradigm for approaching the forbidden phase transition in the one-dimensional Ising model at fixed finite temperature: Single chain in a magnetic field, *Phys. Rev. B* **109**, 214413 (2024).
- [24] W. Yin, Site-decorated model for unconventional frustrated magnets: Ultranarrow phase crossover and spin reversal transition, arXiv:2502.11270 (2025).
- [25] Z. Glumac and K. Uzelac, The partition function zeros in the one-dimensional q-state potts model, *Journal of Physics A: Mathematical and General* **27**, 7709 (1994).
- [26] W. Yin, C. R. Roth, and A. M. Tsvelik, Spin frustration and an exotic critical point in ferromagnets from nonuniform opposite  $g$  factors, *Phys. Rev. B* **109**, 054427 (2024).
- [27] Z.-D. Yu, Y. Zhou, W.-G. Yin, H.-Q. Lin, and C.-D. Gong, Phase competition and anomalous thermal evolution in high-temperature superconductors, *Phys. Rev. B* **96**, 045110 (2017).
- [28] V. J. Emery and S. A. Kivelson, Importance of phase fluctuations in superconductors with small superfluid density, *Nature* **374**, 434 (1995).
- [29] S. Chakravarty, H.-Y. Kee, and K. Volker, An explanation for a universality of transition temperatures in families of copper oxide superconductors, *Nature* **428**, 53 (2004).
- [30] K. Momma and F. Izumi, VESTA 3 for three-dimensional visualization of crystal, volumetric and morphology data, *J. Appl. Crystallogr.* **44**, 1272 (2011).

## END MATTER

### A. AI-Aided Exact Solution for $q = 3$

First of all, OpenAI's latest reasoning model o3-mini-high testified that to the best of its knowledge, the 1D  $J_1$ - $J_2$  Potts model had not been exactly solved.

Next, it was prompted to use the zigzag-ladder version of the 1D  $J_1$ - $J_2$  three-state Potts model. The AI correctly gave

$$H = -J_1 \sum_{n=1}^N \left[ \delta(\sigma_{n,A}, \sigma_{n,B}) + \delta(\sigma_{n,B}, \sigma_{n+1,A}) \right] - J_2 \sum_{n=1}^N \left[ \delta(\sigma_{n,A}, \sigma_{n+1,A}) + \delta(\sigma_{n,B}, \sigma_{n+1,B}) \right], \quad (\text{S1})$$

with periodic boundary conditions  $\sigma_{N+1,A} \equiv \sigma_{1,A}$  and  $\sigma_{N+1,B} \equiv \sigma_{1,B}$ . Here,  $A$  and  $B$  denote the two legs.  $\sigma_{n,A} \in \{1, 2, 3\}$  is the spin variable at site  $n$  on the  $A$  leg.

Then, the AI correctly generated the following expression of the transfer matrix

$$\mathbb{T}'((a, b), (a', b')) = \exp \left\{ \frac{\beta J_1}{2} \left[ \delta(a, b) + \delta(a', b') \right] + \beta J_1 \delta(b, a') + \beta J_2 \left[ \delta(a, a') + \delta(b, b') \right] \right\}, \quad (\text{S2})$$

where  $(a, b)$  with  $a, b \in \{1, 2, 3\}$  is a "rung" state consisting of a spin pair on a rung, and  $(a', b')$  is a neighboring rung state. Let the 9 states of a rung state be ordered as follows:  $(1, 1), (1, 2), (1, 3), (2, 1), (2, 2), (2, 3), (3, 1), (3, 2), (3, 3)$ . With the shorthand notations  $x = e^{\beta J_2}$ ,  $y = e^{\beta J_1/2}$ ,  $z = e^{\beta J_1} = y^2$ , the transfer matrix is given explicitly by

$$\mathbb{T}' = \begin{pmatrix} x^2 y^2 z & xyz & xyz & xy & y^2 & y & xy & y & y^2 \\ xy & x^2 & x & z & xyz & z & 1 & x & y \\ xy & x & x^2 & 1 & y & x & z & z & xyz \\ xyz & z & z & x^2 & xy & x & x & 1 & y \\ y^2 & xy & y & xyz & x^2 y^2 z & xyz & y & xy & y^2 \\ y & 1 & x & x & xy & x^2 & z & z & xyz \\ xyz & z & z & x & y & 1 & x^2 & x & xy \\ y & x & 1 & z & xyz & z & x & x^2 & xy \\ y^2 & y & xy & y & y^2 & xy & xyz & xyz & x^2 y^2 z \end{pmatrix}$$

For the above matrix form of  $\mathbb{T}'$ , the AI was prompted to make sure  $\mathbb{T}'_{27} = \mathbb{T}'_{34} = \mathbb{T}'_{48} = \mathbb{T}'_{62} = \mathbb{T}'_{76} = \mathbb{T}'_{83} = 1$  to correct its mistake and identify the  $\mathcal{S}_3$  symmetry group.

The AI was prompted to block-diagonalize  $\mathbb{T}'$ . It found that  $\mathbb{T}'$  can be block diagonalized to  $\mathbb{T}'_{\text{block}} = U^{-1} \mathbb{T}' U$  with the transformation matrix

$$U = \begin{pmatrix} \frac{1}{\sqrt{3}} & 0 & -\frac{1}{\sqrt{2}} & 0 & 0 & 0 & -\frac{1}{\sqrt{6}} & 0 & 0 \\ 0 & \frac{1}{\sqrt{6}} & 0 & 0 & -\frac{1}{\sqrt{2}} & -\frac{1}{\sqrt{6}} & 0 & 0 & -\frac{1}{\sqrt{6}} \\ 0 & \frac{1}{\sqrt{6}} & 0 & -\frac{1}{\sqrt{2}} & 0 & 0 & 0 & -\frac{1}{\sqrt{6}} & \frac{1}{\sqrt{6}} \\ 0 & \frac{1}{\sqrt{6}} & 0 & 0 & 0 & 0 & 0 & \sqrt{\frac{2}{3}} & \frac{1}{\sqrt{6}} \\ \frac{1}{\sqrt{3}} & 0 & 0 & 0 & 0 & 0 & \sqrt{\frac{2}{3}} & 0 & 0 \\ 0 & \frac{1}{\sqrt{6}} & 0 & 0 & 0 & \sqrt{\frac{2}{3}} & 0 & 0 & -\frac{1}{\sqrt{6}} \\ 0 & \frac{1}{\sqrt{6}} & 0 & 0 & \frac{1}{\sqrt{2}} & -\frac{1}{\sqrt{6}} & 0 & 0 & -\frac{1}{\sqrt{6}} \\ 0 & \frac{1}{\sqrt{6}} & 0 & \frac{1}{\sqrt{2}} & 0 & 0 & 0 & -\frac{1}{\sqrt{6}} & \frac{1}{\sqrt{6}} \\ \frac{1}{\sqrt{3}} & 0 & \frac{1}{\sqrt{2}} & 0 & 0 & 0 & -\frac{1}{\sqrt{6}} & 0 & 0 \end{pmatrix}$$

As a result, the first  $2 \times 2$  block of the resulting block-diagonalized transfer matrix is given by

$$\left(\mathbb{T}'_{\text{block}}\right)_{2 \times 2} = \begin{pmatrix} y^2(x^2z + 2) & \sqrt{2}y(xz + x + 1) \\ \sqrt{2}y(xz + x + 1) & (x + 1)^2 + 2z \end{pmatrix} = \begin{pmatrix} xy^2 & \sqrt{2}y \\ \sqrt{2}y & x + 1 \end{pmatrix}^2, \text{ for } z = y^2,$$

whose larger eigenvalue is  $\lambda$ , the largest eigenvalue of the transfer matrix  $\mathbb{T}'$ .

Finally, the AI was prompted to generate the native Wolfram Mathematica 14.2 code for the above conversation. The task was done in seconds with little need of correction. Nevertheless, the AI failed to generate a workable Mathematica code for general  $q$ . Instead, it warned that the number of permutations in the  $S_q$  symmetry group increases dramatically as  $q$  increases. When pushed, the AI created a few fake Mathematica functions, which ‘‘might be worth implementing,’’ said Yi Yin, Associate Director of Academic Innovation of Wolfram Research, Inc., at its exhibition booth in APS Global Summit 2025.

**Software.** VESTA 3.5.8 [30] was used to plot Fig. 1. Wolfram Mathematica 14.2 was used to plot Figs. 2, 3, S1 and perform brute-force numerical computation of the eigenvalues of the  $q^2 \times q^2$  transfer matrix for  $q^2$  up to 1024 to have verified the exact results.

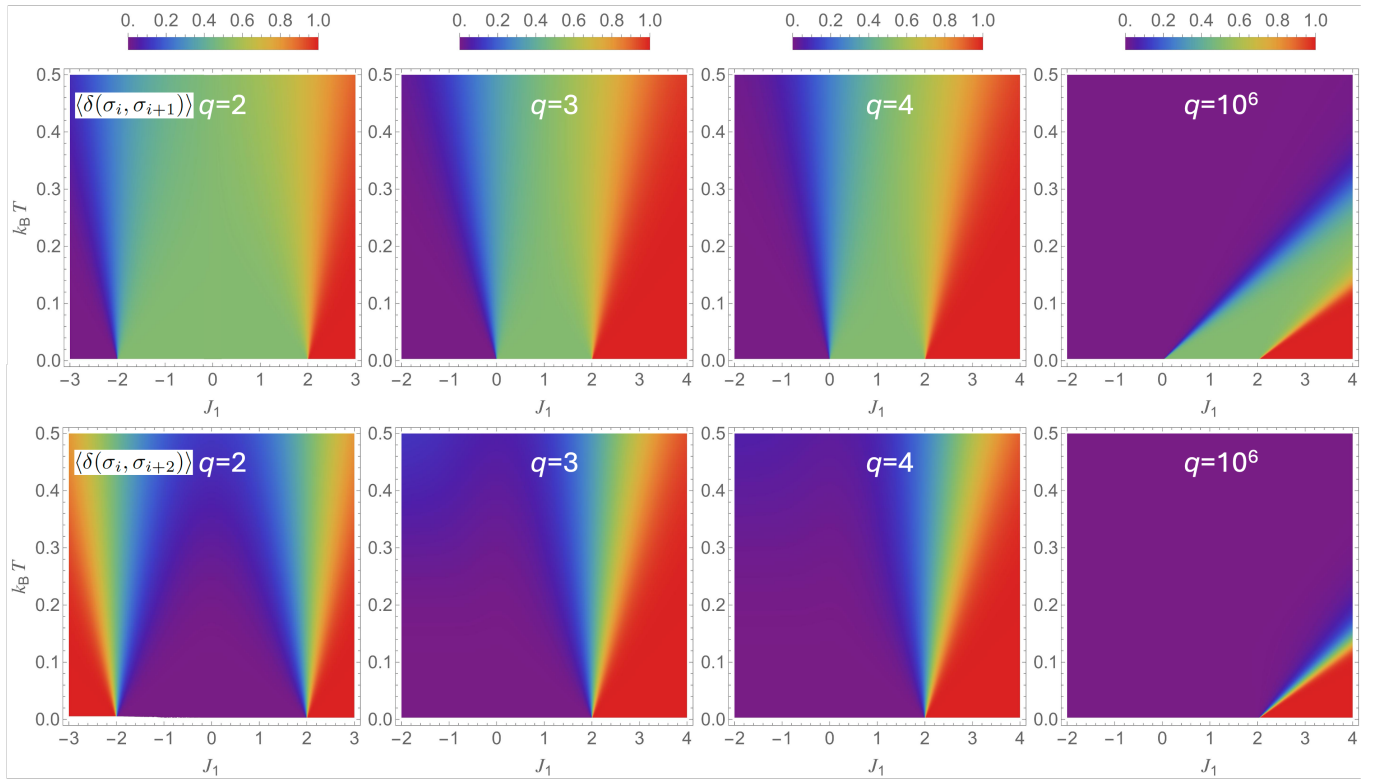


FIG. S1. Phase diagrams in the  $J_1 - T$  plane for  $q = 2, 3, 4$ , and  $10^6$  given by the density plots of  $\langle \delta(\sigma_i, \sigma_{i+1}) \rangle$  (top panels) and  $\langle \delta(\sigma_i, \sigma_{i+2}) \rangle$  (bottom panels).  $-J_2 = 1$  is set as the energy unit.